


Article

Power Split Supercharging: A Mild Hybrid Approach to Boost Fuel Economy

Shima Nazari ^{1,*} , Jason Siegel ², Robert Middleton ² and Anna Stefanopoulou ²

¹ University of California Davis; snazari@ucdavis.edu

² University of Michigan; {siegeljb,rjmidd, annastef}@umich.com

* Correspondence: snazari@ucdavis; Tel.: +1-530-752-5801

Abstract: This work studies a novel low voltage (<60 V) hybrid system that supports engine boosting and downsizing in addition to start-stop, regenerative braking, and constrained torque assist/regeneration. The hybrid power split supercharger (PSS) shares a 9 kW motor between supercharging the engine or providing hybrid functionalities through a planetary gear set, a brake and a bypass valve. The PSS operation is limited to only one of the parallel hybrid or boosting modes at a time, necessitating a highly optimized decision making algorithm to select the device mode and power split ratio. In this work an adaptive equivalent consumption minimization strategy (A-ECMS) is developed for energy management of the PSS. The A-ECMS effectiveness is compared against a dynamic programming (DP) solution with full drive cycle preview through hardware-in-the-loop experiments on an engine dynamometer testbed. The experiments show that the PSS with A-ECMS reduces a vehicle fuel consumption by 18.4% over standard FTP75 cycle compared to a baseline turbocharged engine, while global optimal DP solution decreases the fuel consumption by 22.8% compared to baseline.

Keywords: Energy management, hybrid electric vehicle, powertrain electrification, equivalent consumption minimization, supercharging, hardware-in-the-loop experiments

1. Introduction

Hybrid Electric Vehicles (HEVs) are one of the promising solutions for reducing carbon emissions of the transportation sector. During the past two decades many different architectures for hybridized powertrains have emerged [1]. Unfortunately, despite their relative technology maturity and their proven effectiveness in reducing fuel consumption, the market penetration of HEVs is still poor [2]. The main factor for low sales rates is the higher initial cost of these vehicles compared to traditional vehicles with only Internal Combustion Engines (ICEs). In contrast to expensive full HEVs, which use high voltage/power electric machines and electronics, this work focuses on an economic low voltage system, called a Power Split Supercharger (PSS). Figure 1 shows a schematic view of the PSS in a vehicle configuration.

The PSS, configured with a 9 kW 48 V motor, can switch between providing power to the crankshaft (for start-stop, regenerative braking or torque assist) and variable speed supercharging. Conventional low-voltage hybrids have to couple with a large Naturally Aspirated (NA) ICE or a boosted smaller engine, because the limited torque of the motor cannot augment the torque of a small NA engine to full performance. However, the boosting capability of the PSS allows it to be used with a small engine and benefit from engine downsizing in addition to hybridization.

The electric motor and the planetary gear set decouple the PSS produced boost pressure from the crankshaft speed, resulting in a fast torque response and improved vehicle drive-ability compared to traditional boosting devices, such as turbochargers or mechanical superchargers. Flexible supercharging can also be achieved with an electric supercharger such as the HyBoost system from Valeo [3]. However, powering the supercharger solely with electricity necessitates a larger battery and motor, leading to a higher system cost. Figure 2(a) shows the supercharger required mechanical power

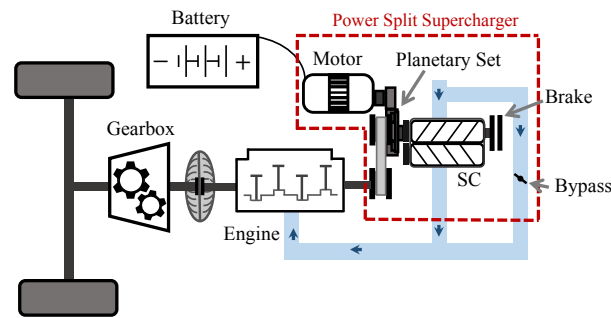


Figure 1. Powertrain schematic with a power split supercharger.

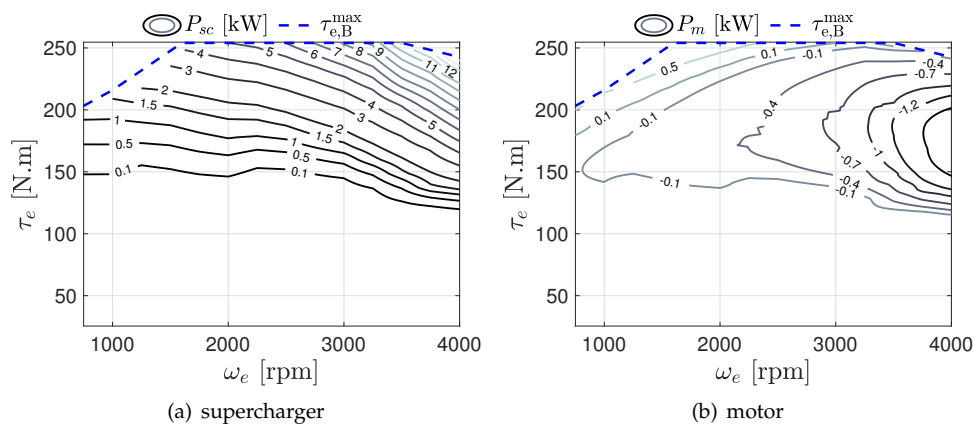


Figure 2. (a) Supercharger mechanical power, (b) corresponding motor power in the PSS system, both for a 1.6 L gasoline engine.

in a 1.6L gasoline engine studied here and Figure 2(b) shows the corresponding motor power in the PSS system for different engine speeds and torques. While for the range of operating points shown the supercharger power is as high as 15 kW, most of this power is supplied by the engine crankshaft and in every operating condition either a small portion of the power comes from the motor or the motor is slightly generating. This characteristic is especially useful for scenarios such as hill climbing, shown in Figure 3, where the supercharger has to provide a continuous boost pressure due to the high requested torque. For the simulated example shown in Figure 3, vehicle cruising at 110 km/h with a road grade of 5° for 20 minutes, a small SUV with the PSS would slightly charge a 2.5 kW.h battery, while a purely electric supercharger (eSC) will completely deplete the battery, as demonstrated in Figure 2(b). The modeled vehicle and engine are explained in further detail in next sections.

This electric power and energy accessibility problem has pushed the vehicle manufacturers to use electric superchargers in combination with a turbocharger, examples of which are Volvo T6 and T8 engines [4]. In these powertrains the turbocharger can be used during steady state and the supercharger can make the transients faster. The PSS system, however, can be used as a stand-alone boosting device reducing the system cost in addition to enabling hybrid functionalities such as regenerative braking and start-stop. This work focuses on developing an online energy management system for an engine equipped with a PSS and experimental validation of the fuel economy benefits. The energy management system of the PSS has to decide where and by how much to supply the limited available electric power, either to the air path via the supercharger or directly to the crankshaft.

Energy management systems of HEVs fall into the two main categories of rule-based approaches and optimization-based approaches [5,6]. Rule-based methods are static controllers that are developed offline based on heuristics or approximations to optimization results. Thermostatic control, which

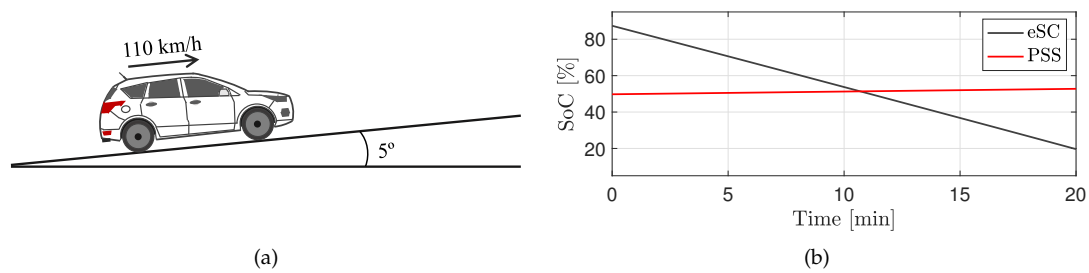


Figure 3. (a) Vehicle climbing a 5° hill at 110 km/h, (b) a 2.5 kWh battery state of charge (SoC) variation for the vehicle with PSS compared to the same vehicle with an electric supercharger (eSC).

turns the engine on and off based on the battery state of charge, is an example of rule-based control for a series HEV [7]. Load-leveling, which uses only the motor at low load, the engine at medium load and both at high load, is an example of a rule-based approach for a parallel HEV [8]. These controllers are based on simple concepts and are easily implementable. However, they do not exploit the full potential of the system for fuel consumption reduction and are not reusable for a different objective or powertrain configuration.

Optimization-based methods on the other hand, use physics-based modeling and optimization techniques to minimize a cost function that can include different performance metrics such as fuel consumption or emissions. The objective cost can be minimized instantaneously, like the equivalent consumption minimization method [9], or over some receding horizon, such as with Model Predictive Control (MPC) [10], or over the full driving profile, as in Dynamic Programming (DP) [11,12]. The methods that optimize the fuel consumption over the full driving profile give the global optimum solution, but they are prohibitively computationally expensive while also requiring knowledge of future driver demands. Nevertheless, they provide a benchmark for comparing other energy management systems and give insight into optimal policies.

The global fuel consumption minimization for a hybrid electric vehicle equipped with a power split supercharger under a charge sustaining constraint was previously formulated and solved using Dynamic Programming (DP) by the authors [13] and a simple online energy management system based on Equivalent Consumption Minimization Strategy (ECMS) was also previously presented [14] and was tested in simulation. This work extends our previous efforts by developing an Adaptive-ECMS (A-ECMS) and documenting the fuel economy benefits of the PSS through advanced hardware-in-the-loop (HIL) experiments. The main contributions of this work are: first, an Adaptive-ECMS energy management system is introduced to select the PSS mode and its power split ratio, second, the implementation of the hardware-in-the-loop experiments is described in detail and some practical challenges are explained and finally, the effectiveness of the developed controllers and the fuel consumption reduction of the new engine compared to a baseline turbocharged engine is quantified on the FTP75 standard drive cycle.

After introducing the utilized hardware and models, the global fuel consumption minimization problem is described briefly. An ECMS is formulated for selecting the PSS mode and its power split ratio in section 3.2 and the adaptive ECMS is described in section 3.3. Section 4 presents the engine dynamometer experimental testbed and the details of HIL implementation. The experimental demonstration of fuel economy results and PSS operation are shown in section 5 and the paper concludes with the main findings of the work.

2. Experimental Hardware and Model Framework

The baseline engine is a 1.6 liter, 4 cylinder four stroke gasoline fueled turbocharged Spark Ignition Direct Injection (SIDI) engine, patterned off a Ford EcoBoost engine. The PSS is coupled with the engine after removing the turbocharger. Figure 1 shows a schematic view of the engine with the PSS in a vehicle configuration. The PSS is configured with a motor, a roots blower, a planetary gear set, a

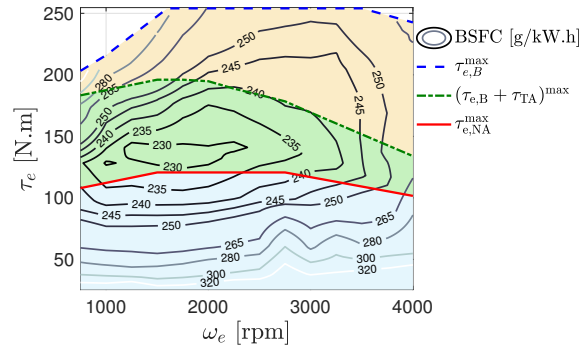


Figure 4. Brake Specific Fuel Consumption (BSFC) for engine with the Power Split Supercharger (PSS) along with the maximum engine torque at boosting mode, $\tau_{e,B}^{\max}$, the powertrain maximum torque at torque assist mode, $(\tau_{e,NA} + \tau_{TA})^{\max}$, and the naturally aspirated engine maximum torque, $\tau_{e,NA}^{\max}$.

brake, and a bypass valve. The ring gear is connected to the motor, the sun gear is connected to the supercharger, while the carrier is connected to the engine crankshaft via a set of belt and pulleys. By controlling the brake and the bypass valve this device can operate in two distinct modes. When the brake is released and the bypass is closed, the motor can control the supercharger speed and hence the boost pressure independently of the engine speed. This mode is called the boosting mode. When the supercharger is locked and bypassed, the motor can draw/supply torque to the crankshaft, similar to a parallel hybrid powertrain. This mode is called the torque assist mode in this work regardless of the torque direction. The engine fuel consumption map, shown in Figure 4, is produced using a high fidelity GT-Power model, which is described in detail and validated against engine dynamometer experiments elsewhere [15]. In Figure 4 $\tau_{e,B}^{\max}$ is the maximum engine torque when the PSS is in boosting mode, $\tau_{e,NA}^{\max}$ is the maximum torque for the NA engine and $(\tau_{e,NA} + \tau_{TA})^{\max}$ is the powertrain maximum torque in torque assist mode (maximum motor torque added to the crankshaft).

The modeled vehicle is a MY2015 Ford Escape with 6 speed automatic transmission. The drivetrain model includes a transmission, a friction clutch in parallel with a torque converter and crankshaft dynamics. The individual models of each component along with the transmission and clutch control strategy are described in detail elsewhere [16]. The driver model is a Proportional+Integral (PI) controller that switches gains based on a 1 second preview of the vehicle acceleration and the tracking error. A 1.2 kWh lithium ion battery is assumed for the vehicle. An Open Circuit Voltage with a Resistance (OCV-R) is used to model the battery and compute its state of charge dynamics detailed in [13]

3. Energy Management System

3.1. Global Fuel Consumption Minimization

The global fuel consumption minimization problem for a vehicle equipped with a PSS was formulated and solved using Dynamic Programming (DP) by the authors elsewhere [13,17]. In this work the online energy management system is compared to DP results to determine the sub optimality of the solution, hence only a brief summary of the DP formulation is provided. The cost function in the global fuel consumption minimization problem penalizes the fuel flow rate, the gear shifts, the engine cranking (for start-stop) and the PSS mode as follows:

$$\min \left\{ \sum_{k=1}^N \left(\dot{m}_f(k) T_s + \alpha |n_g(k) - n_g(k-1)| + \beta (\max(x_e(k) - x_e(k-1), 0)) + \lambda (1 - u_{br}(k)) \right) \right\} \quad (1)$$

in which \dot{m}_f is the fuel flow rate, n_g is the gear number, x_e is the engine on/off state and u_{br} is the PSS mode. The PSS mode is denoted by its brake position in this work, where $u_{br} = 1$ represents the

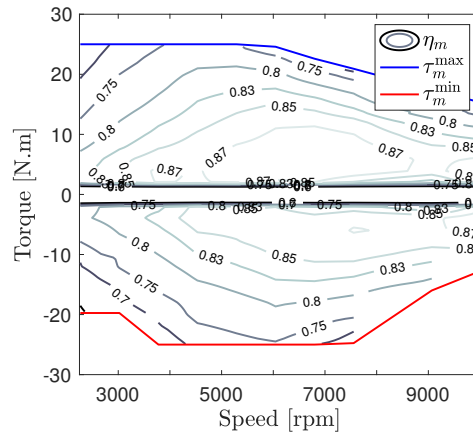


Figure 5. Experimentally generated motor and gear set map.

torque assist mode and $u_{br} = 0$ the boosting mode. The coefficient α controls the gear shift frequency and λ is a very small number to keep the PSS in torque assist mode as the default mode. This term only plays a role when neither supercharging nor torque assist are used. The variable k refers to k^{th} step time, the problem horizon, N , is the full drive cycle and T_s is the problem sampling time equal to 1 second. The problem inputs are the commanded torque assist from the electric motor, gear shift command, the PSS mode, and the engine on/off command. The modeled system states include the battery state of charge the gear number, and the engine on/off state. The latter two are modeled as states only to be penalized in the cost function. This problem was solved using a MATLAB based dynamic programming function. Full details are provided in the original work [17].

In the prior work the manufacturer map for the electric motor was used to estimate the fuel economy and no loss was assumed for the planetary gear set and pulleys. However, the experiments showed that both the motor efficiency and its torque limits are different from the manufacturer map. Hence, new experimentally validated maps were produced to update the results in this work. Figure 5 shows the measured efficiency from/to the electric power, measured by an AVL battery emulator, to/from the engine-dynamometer crankshaft, measured using a torque meter. The maximum and minimum motor torque limits are also represented. Compared to the prior maps, the losses are up to 15% more, specially at low speed and negative torques. The minimum motor torque is also slightly higher at lower engine speeds. Both of these reduce the recuperated power from regenerative braking during a cycle. The DP results presented later in Table 1 are updated with the new map.

3.2. Equivalent Consumption Minimization

The equivalent consumption minimization proposed by Paganelli [9,18] minimizes the instantaneous sum of the engine and motor fuel flow rate by using a factor to convert the electric energy consumption to an equivalent fuel flow rate. The motor torque in ECMS is computed as follows:

$$\tau_m = \underset{\tau_m}{\operatorname{argmin}} (\dot{m}_f(\tau_e, \omega_e) + \alpha_{eq} P_m(\tau_m, \omega_m)) \quad (2)$$

where τ_m is the motor torque, ω_m is the motor speed, τ_e is the engine torque, ω_e is the engine speed and α_{eq} is the equivalence factor. The Energy Management System (EMS) of an engine with a PSS is different from a conventional HEV because it has to decide on the PSS mode first and if the torque assist mode is selected then the EMS has to determine the optimum motor torque to minimize the powertrain fuel consumption. Note that the motor torque is an optimization parameter in torque assist mode but not in the boosting mode, during which the motor controls the boost pressure and hence the engine torque.

When the requested crankshaft torque, τ_{cr}^d , is less than the naturally aspirated torque limit of the engine, $\tau_{e,NA}^{\max}$ (the blue area in Figure 4) it is fuel optimal to brake and bypass the supercharger, hence

the PSS should be in torque assist mode. On the other hand, when the requested torque is larger than $\tau_{e,NA}^{\max}$ plus the maximum torque assist from the motor on the crankshaft, $(\tau_{e,NA} + \tau_{TA})^{\max}$ (the yellow area in Figure 4) the powertrain can only supply the requested torque through supercharging, hence the PSS must be in boosting mode. Finally, when the requested torque is larger than $\tau_{e,NA}^{\max}$ and smaller than the powertrain torque limit in torque assist mode (green area in Figure 4) the requested torque can be realized through either mode. In this work a consumption minimization rule that selects the PSS mode for minimizing the sum of the engine and the motor fuel flow rate is introduced:

$$u_{br} = \begin{cases} 0 & \text{if } \tau_{cr}^d > (\tau_{TA} + \tau_{e,NA})^{\max} \\ 1 & \text{if } \tau_{cr}^d \leq \tau_{e,NA}^{\max} \\ \text{argmin}_{u_{br}=0,1}(\dot{m}_{f,eq}) & \text{otherwise} \end{cases} \quad (3)$$

where u_{br} is the PSS mode for consumption minimization and $\dot{m}_{f,eq}$ is the equivalent fuel flow rate of the engine and motor, computed for each mode as:

- Boosting mode ($u_{br} = 0$):

$$\dot{m}_{f,eq} = \dot{m}_f(\tau_e^d, \omega_e) + \alpha_{eq} P_m(\tau_e^d, \omega_e) \quad (4a)$$

$$\tau_e^d = \tau_{cr}^d \quad (4b)$$

Equation (4b) indicates that during boosting mode the entire crankshaft requested torque has to be supplied by the engine.

- Torque assist mode ($u_{br} = 1$):

$$\dot{m}_{f,eq} = \min_{\tau_m^d} \left(\dot{m}_f(\tau_e^d, \omega_e) + \alpha_{eq} P_m(\tau_m^d, \omega_m) \right) \quad (5a)$$

$$\tau_e^d = \tau_{cr}^d - \tau_{TA}^d \quad (5b)$$

$$\tau_m^d = \frac{g_R}{n_{im} n_{ri} (g_S + g_R)} \tau_{TA}^d \quad (5c)$$

where τ_{TA} is the torque assist from the motor on the crankshaft related to the motor torque through (5c), g_S is the sun gear teeth number, g_R is the ring gear teeth number, n_{im} is the idler to motor gear ratio and n_{ri} is the ring to idler gear ratio. The superscript d refers to the desired or commanded values.

During boosting mode the planetary gear set and the motor decouple the supercharger produced boost pressure from the engine operating speed. The engine losses are minimized by utilizing Wide Open Throttle (WOT) in these operating points. Employing a WOT strategy, the motor power for supercharging is a function of the engine operating point during steady state, shown in Figure 2(b). This steady state map is used to compute the equivalent fuel consumption of the engine in boosting mode. During torque assist mode, the motor supplies part of the torque demand, Equation (5b), and for a given equivalence factor, the motor torque should be determined to minimize the equivalent fuel flow rate of the engine and the motor, similar to a traditional ECMS problem. The solution to Equations (2) and (3) is computed for various values of the equivalence factor. Figures 6(a), 6(b), and 6(c) show the solution to Equation (3) for equivalence factors of 0.13, 0.18 and 0.23 kg/kWh, respectively. The green color in these plots indicates boosting mode, while the red color shows torque assist mode. Figures 7(a), 7(b), and 7(c) present the optimum motor torque during torque assist mode generated from (2) for the same equivalence factors.

The equivalence factor represents the relative value of the electric power. A smaller equivalence factor uses the torque assist mode more often and uses the motor to assist the crankshaft over a larger operating region (more red color in Figure 6(a) and 7(a)). A higher equivalence factor increases the

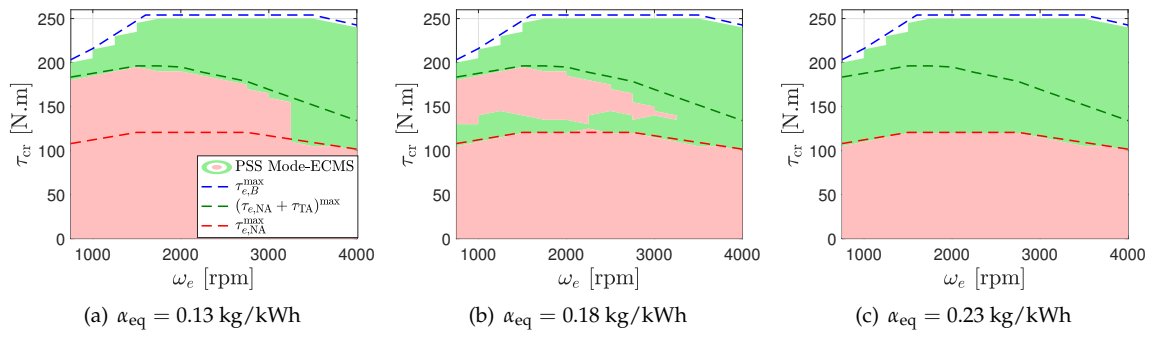


Figure 6. ECMS generated PSS mode for different equivalence factors, the green color stands for boosting mode and the red color shows torque assist mode. (a) $\alpha_{eq} = 0.13$ kg/kWh, (b) $\alpha_{eq} = 0.18$ kg/kWh, (c) $\alpha_{eq} = 0.23$ kg/kWh. Increasing the equivalence factor shifts the optimal strategy from torque assist to favor boosting mode.

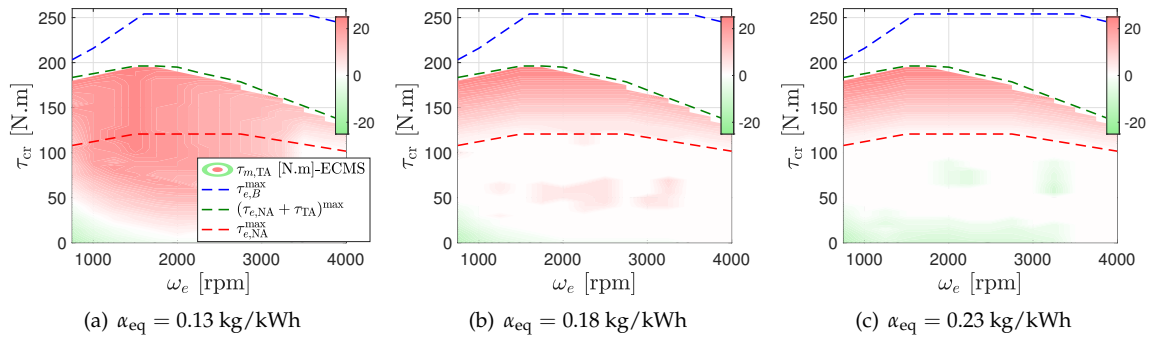


Figure 7. ECMS generated motor torque during torque assist mode for different equivalence factors (a) $\alpha_{eq} = 0.13$ kg/kWh, (b) $\alpha_{eq} = 0.18$ kg/kWh, (c) $\alpha_{eq} = 0.23$ kg/kWh.

penalty for electric power, which causes the ECMS controller to use the boosting mode more often in Figures 6(b) and 6(c), while also using the motor to generate more energy often at low loads (more green color in Figure 7(b) and 7(c)).

3.3. Adaptive-ECMS

The traditional ECMS method needs tuning the equivalence factor offline for every driving profile to ensure that the battery state of charge remains within the desired/operational limit. However, in real world applications the future velocity profile is not known. Therefore, it is necessary to tune the ECMS factor in real time to ensure acceptable operation of the energy management system, especially when starting from an unfavorable initial condition. Adaptive ECMS (A-ECMS) adjusts the equivalence factor based on drive cycle prediction, driving pattern recognition, or feedback from the battery state of charge [19]. In this work a modification of the approach that uses the SoC feedback [20] is adopted. The equivalence factor is adjusted as:

$$\alpha_{eq}(k) = \begin{cases} 0.25 & \text{if } \text{SoC} < 40\% \\ 0.10 & \text{if } \text{SoC} > 60\% \\ \max\left(\min\left(\alpha_{eq}(k-1) + q(\text{SoC}(k) - \text{SoC}(k-1)), 0.25\right), 0.10\right) & \text{otherwise} \end{cases} \quad (6)$$

where q is a constant coefficient. The sampling time for equation (6) is chosen as 15 seconds.

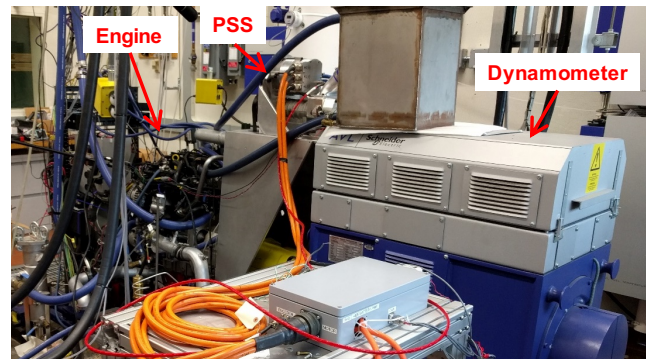


Figure 8. Engine-dynamometer experimental testbed.

4. Experimental Setup

4.1. Testbed

Figure 8 shows a picture of the engine-dynamometer experimental testbed, which includes an AVL AC transient dynamometer, an instrumented 1.6 L Ford EcoBoost engine and the power split supercharger by EATON. An AVL SESAM-FTIR emission measurement bench is used to measure exhaust gas species and calculate fuel flow rate along with a hot wire air flow rate meter. An AVL Battery Simulator is used to power the PSS and measure the motor current and voltage. A Rapid Prototyping Electronic Control System (RPECSTM) from Southwest Research Institute (SwRI) is used to integrate all engine controllers, the online energy management system, and implement real-time vehicle and driver models.

4.2. Implementing A-ECMS and Hardware-in-the-Loop Experiments

In the hardware-in-the-loop (HIL) experiments the engine and the PSS are the physical hardwares and the vehicle, the driver, and the battery are models coded in RPECSTM. The AC dynamometer is programmed to play the role of the vehicle body and follow a drive cycle speed profile. In these experiments the driver model issues an accelerator or brake pedal based on the vehicle velocity tracking error. From this command the energy management system and the low level controllers compute the actuator positions for the engine, dynamometer and the PSS, including the throttle position (u_{θ}^d), motor torque (τ_m^d), the PSS brake command (u_{br}^d), the supercharger bypass command (u_{bp}^d), and the engine speed (ω_e^d). The produced crankshaft torque ($\hat{\tau}_{crk}$) is measured and fed back into the vehicle longitudinal dynamics to calculate the next vehicle speed. This feedback system, presented also in Figure 9, permits velocity tracking and an accurate drive cycle fuel economy measurement. Note that the AC dynamometer can track either a desired speed or a desired torque profile. The torque tracking mode is not always safe because in this case the crankshaft speed is determined by the torque balance between the engine and the dynamometer. Operating in this mode in case of a subsystem failure, communication delay, or software bug can result in over speeding the engine, damage or complete destruction. Therefore, in this work the dynamometer is always used in the speed control mode and as shown later in the experimental results the dynamometer controller does an impeccable job in tracking the engine speed set point. The following sections present HIL implementation for the two propulsion modes, locked and unlocked torque converter. All models and the energy management system are implemented in a 5 ms loop in RPECS.

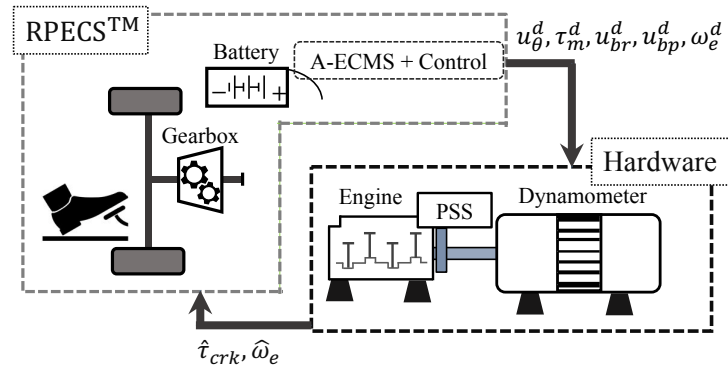


Figure 9. Hardware-in-the-loop (HIL) implementation.

4.2.1. Hardware-in-the-Loop Implementation for Locked Torque Converter

When the Torque Converter (TC) is locked the vehicle speed is computed from the longitudinal vehicle dynamics and the measured crankshaft torque as follows:

$$M \frac{d}{dt} v = F_t - F_b - F_l \quad (7a)$$

$$F_t = i_g \hat{\tau}_{crk} - \tau_{loss} \quad (7b)$$

$$\omega_e^d = \frac{v}{i_g R_w} \quad (7c)$$

where M is the vehicle mass, v is the vehicle velocity, F_t is the traction force, F_b is the braking force, F_l is the road load, i_g is the gear ratio, τ_{loss} is torque loss in the transmission, R_w is the wheel radius, and ω_e^d is the engine speed computed from the vehicles speed and fed back into the dynamometer. The details of the vehicle and transmission models are presented elsewhere [15].

The requested tractive torque, τ_{trc}^d , when the accelerator pedal is active is linearly mapped to the pedal position, u_{acc} :

$$\tau_{trc}^d = u_{acc}(\tau_{e,B}^{\max} - \tau_e^{\min}) + \tau_e^{\min} \quad (8)$$

where τ_e^{\min} is the minimum engine torque and $\tau_{e,B}^{\max}$ is from Figure 4. The requested braking torque on the gearbox inlet shaft, τ_{brk}^d , is computed from the brake pedal position, u_{brk} produced by the driver model:

$$\tau_{brk}^d = \frac{u_{brk} \tau_{brk}^{\max}}{\gamma} \quad (9)$$

where τ_{brk}^{\max} is the maximum braking torque on the wheels and γ is the gear ratio in the gearbox.

The PSS optimal mode, u_{br}^d , during traction (which is $\tau_{cr}^d > 0$) and the optimum motor torque in torque assist mode, $\tau_m^{d,TA}$, are computed offline and stored in look up tables based on the requested crank torque, the measured engine speed, and the equivalence factor:

$$u_{br}^d = \Gamma(\tau_{crk}^d, \hat{\omega}_e, \alpha_{eq}) \quad (10a)$$

$$\tau_m^{d,TA} = \Lambda(\tau_{crk}^d, \hat{\omega}_e, \alpha_{eq}) \quad (10b)$$

The desired engine torque is:

$$\tau_e^d = \begin{cases} \tau_{crk}^d & \text{if } u_{br}^d = 0 \\ \tau_{crk}^d - \tau_m^{d,TA} \frac{(g_R + g_S)n_{im}n_{ri}}{g_R} & \text{if } u_{br}^d = 1. \end{cases} \quad (11)$$

Finally the desired intake manifold pressure is computed from the engine speed and the desired engine torque:

$$p_{im}^d = \Xi(\tau_e^d, \omega_e). \quad (12)$$

When the desired manifold pressure is less than the ambient pressure the supercharger is bypassed ($u_{bp}^d = 1$) and the intake throttle is used to control the intake manifold pressure, while when the desired intake manifold pressure is higher than the ambient pressure the throttle is wide open and the supercharger speed is controlled by the motor to achieve the desired intake manifold pressure. Both the throttle controller and the supercharger speed controller are PI controllers with feedforward. The supercharger speed controller has an inner PI controller to manipulate the motor torque to achieve the desired supercharger speed. The details of the low level controllers are presented elsewhere [15].

The motor torque during regenerative braking, $\tau_m^{d,Reg}$, is computed by:

$$\tau_m^{d,Reg} = \max(\tau_{crk}^d \frac{g_R}{(g_R + g_S)n_{im}n_{ri}}, \tau_m^{\min}) \quad (13)$$

where τ_m^{\min} is the minimum motor torque shown in Figure 5. The PSS mode is set to torque assist mode during braking. Note that Equation (13) is the solution to Optimization (2). Finally, the commanded motor torque, τ_m^d , comes from either the PI controller ($\tau_m^{d,PI}$), regenerative braking, or the torque assist (from A-ECMS) depending the PSS mode and the requested tractive torque sign:

$$\tau_m^d = \begin{cases} \tau_m^{d,PI} & \text{if } u_{br}^d = 0 \\ \tau_m^{d,TA} & \text{if } u_{br}^d = 1, \tau_{trc}^d \geq 0 \\ \tau_m^{d,Gen} & \text{if } u_{br}^d = 1, \tau_{trc}^d < 0 \end{cases} \quad (14)$$

4.2.2. Hardware-in-the-Loop Implementation for Unlocked Torque Converter

When the torque converter is unlocked, there is no mechanical coupling between the engine and the wheels. However, in order to use the dynamometer in the speed control mode with an unlocked torque converter, it is assumed that the engine speed is equal to its idling speed when the TC unlocks ($\omega_e^d = \omega_{e,idle}$). The minimum engine torque to hold the idle speed is calculated from the torque converter K-factor (K) and Torque Ratio (TR), which are functions of turbine to pump Speed Ratio (SR):

$$SR = \frac{\omega_{tct}}{\omega_{tcp}} \quad (15a)$$

$$\tau_{tcp} = \left(\frac{\omega_{tcp}}{K}\right)^2 \quad (15b)$$

$$\tau_{tct} = \tau_{tcp} \times TR \quad (15c)$$

where ω_{tct} is the torque converter turbine speed, τ_{tct} is the turbine torque, τ_{tcp} is the pump torque, and ω_{tcp} is the pump speed. Given that ω_{tcp} is equal to the engine idling speed when the torque converter unlocks, the minimum torque on the crankshaft when the turbine speed drops to less than engine

idling speed can be computed as a function of turbine speed, $\tau_{tcp}^*(\omega_{tct})$. Accordingly, the minimum torque on the crankshaft, τ_{crk}^{\min} , is computed by:

$$\tau_{crk}^{\min} = \begin{cases} \tau_{tcp}^*(\omega_{tct}) & \text{if } \omega_{tct} \leq \omega_{e,idle} \\ -\infty & \text{otherwise.} \end{cases} \quad (16)$$

The requested torque on the crankshaft is:

$$\tau_{crk}^d = \max(\tau_{trc}^d, \tau_{brk}^d, \tau_{crk}^{\min}). \quad (17)$$

Equation (17) imposes some positive torque demand on the crankshaft at low vehicle speed to maintain the engine idling speed and it disables regenerative braking under these conditions. Similar to the locked torque converter case, equations (10) - (12) and (14) are used to determine u_{θ}^d , τ_m^d , u_{bp}^d , and u_{br}^d in this mode. The engine speed is set equal to the idling speed, $\omega_e^d = \omega_{e,idle}$, and (7b) has to be corrected to include the torque converter torque ratio,

$$F_t = i_g \hat{\tau}_{crk} \times TR - \tau_{loss}. \quad (18)$$

4.2.3. Engine Start/Stop

It is not possible to test engine start-stops with a dynamometer, because in a vehicle the engine is connected to the transmission and the transmission clutch is open during engine starts, while on the engine dynamometer the engine is permanently connected to the dynamometer with a large inertia. To emulate the start-stop behavior the stopped portions of the drive cycle, where the engine is turned off, are removed from the velocity profile for the vehicle with the PSS and a fuel penalty is added for each start-stop event. The next section shows the resulted velocity profiles in addition to other experimental results.

5. Experimental Results

Figure 10 shows the velocity tracking for FTP75 drive cycle from the HIL experiments for the baseline turbocharged engine and the engine when the PSS replaces the turbocharger. In addition to the vehicle speed and reference speed, v^{ref} , the standard minimum velocity threshold, v^{\min} , is also plotted, showing that both engines successfully follow the cycle profile. The following sections document the fuel consumption and PSS operation details during the HIL experiments.

5.1. Fuel Consumption Reduction with PSS

Table 1 summarizes the experimental Fuel Consumption (FC) results along with the predicted global minimum fuel consumption, produced with Dynamic Programming (DP) and a simplified vehicle model. The gearshifts of the baseline turbocharged engine are also optimized by DP in results shown in the first row of Table 1. The same gearshift strategy is used for the turbocharged engine and the engine with PSS during experiments. DP predicts that the engine with the PSS consumes 22.8% less fuel compared to the turbocharged engine. The HIL experiments were repeated 3 times for the PSS and 2 times for the baseline turbocharged engine and the mean FC values are reported in the table. The FC values varied from 5.92 to 5.99 l/100km for the engine with PSS and from 7.20 to 7.37 l/100km for turbocharged engine. The HIL experiments show that the engine with the PSS consumes 18.4% less fuel compared to the baseline turbocharged engine on average, which is only 4.4% higher than the global minimum FC from DP. This result substantiates the effectiveness of the implemented energy management system considering that A-ECMS does not use any preview information and only minimizes its cost function at a current time step. There is some offset between the absolute values

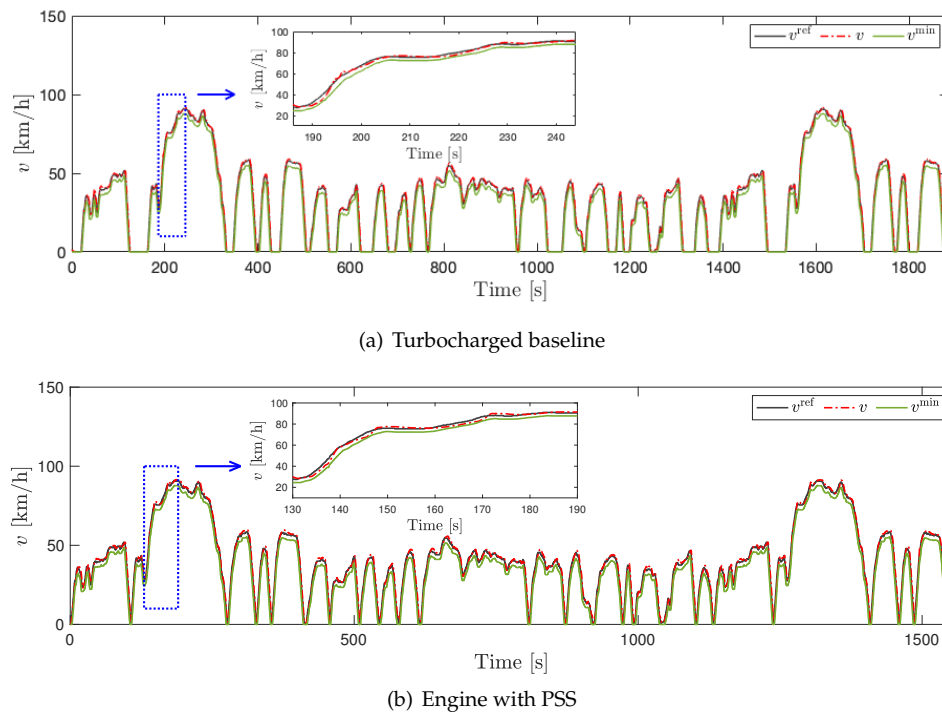


Figure 10. Velocity tracking during hardware-in-the-loop experiments, (a) vehicle with turbocharged engine, (b) vehicle with the PSS, stopped portions of the cycle removed to emulate start-stop.

Table 1. Drive cycle fuel consumption results for Ford Escape MY2015.

Powertrain	Result	Energy	FC	ΔFC	ΔSoC
	Type	Management	[L/100 km]	[%]	[%]
Turbocharged	Simulation	DP	6.76	-	-
Engine + PSS	Simulation	DP	5.22	22.8	0.0
Turbocharged	Experiment	-	7.29	-	-
Engine + PSS	Experiment	A-ECMS	5.95	18.4	1.1

of FC in simulations versus experiments. The reason is that the simulations use a fuel consumption map produced by GT-Power simulations, which is shown to accurately predict the fuel consumption variation with load and speed and between different engine configurations, but has a constant offset compared to the experimentally measured fuel consumption [15].

Figure 11(a) shows the battery State of Charge (SoC) variation during the HIL experiment. Starting from 50% SoC, the battery SoC maintained between 44% to 51% during the experiment, showing the possibility of further battery size and system cost reduction. Figure 11(b) shows the equivalence factor. The adaptation rule (6) can keep the SoC between 40% and 60%, but still the initial value of $\alpha_{eq}(0)$ was tuned to get a final SoC value close to 50%. Finally, the fuel mass is corrected as follows to account for the small ΔSoC between the start and end of the cycle,

$$W_f^{cor} = W_f + UC_n \bar{\alpha}_{eq} \Delta SoC \quad (19)$$

where W_f is the fuel mass, W_f^{cor} is the corrected fuel mass, U is the battery open circuit voltage, C_n is the battery capacity, and $\bar{\alpha}_{eff}$ is the average equivalence factor during the experiment from Figure 11(b).

5.2. Power Split Supercharger Operation During a Transient Drive Cycle

This section presents the details of the hardware and energy management system operation during the HIL experiments. Figure 12 shows the intake manifold pressure, p_{im} . Figure 12(a) shows

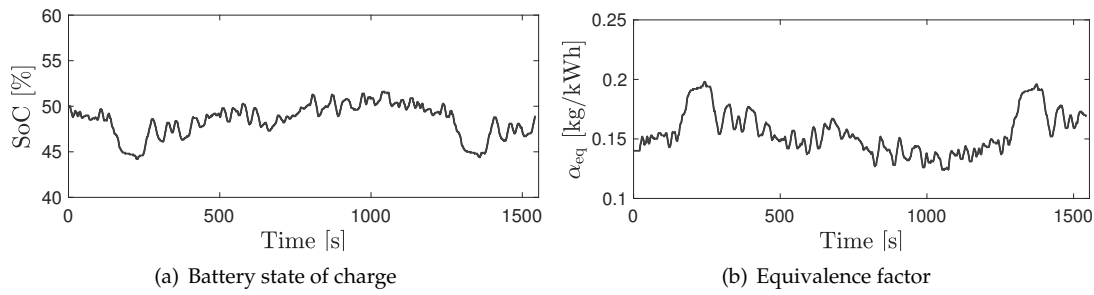


Figure 11. The battery state of charge and A-ECMS equivalence factor variation during experiments, (a) state of charge, (b) equivalence factor

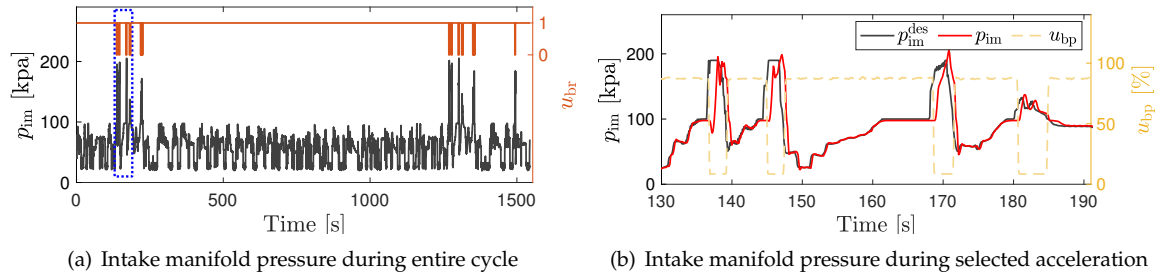


Figure 12. Intake manifold pressure during FTP75 cycle, (a) intake manifold pressure and PSS mode over the entire cycle, (b) intake manifold pressure, desired intake manifold pressure, and supercharger bypass during $t = 130$ s to $t = 190$ s.

p_{im} over the entire cycle along with the PSS brake position. The intake manifold pressure increases to more than the ambient pressure (around 100 kpa) only during few instances, which correspond to vehicle accelerations where the PSS switches to boosting mode ($u_{br} = 0$). Figure 12(b) shows p_{im} variation during a portion of the cycle in more detail (marked with blue square in Figures 10(b) and 12(a)) on top of the desired signal value, p_{im}^{des} , and the supercharger bypass valve position. As mentioned before when p_{im}^{des} is less than the ambient pressure, the supercharger is bypassed and the throttle controls p_{im} and hence the air flow into the engine, while when p_{im}^{des} increases to more than the ambient pressure the throttle wide opens, the bypass valve closes and the supercharger (manipulated by the motor) controls p_{im} . With the current controller gains the 0→90% response time to achieve full boost is around 1 s, but it can be reduced to around 0.7 s with more rigorous calibration and gain scheduling.

Figure 13 shows the engine speed, the motor speed and the supercharger brake position for the same portion of drive cycle. The motor speed is multiplied by $\frac{R}{n_{im}n_{ri}(g_R + g_S)}$, which corresponds to the gear ratio between the motor and crankshaft when the supercharger is locked. During the boosting mode the supercharger speed, ω_{sc} , is related to the motor and crankshaft speed by

$$\omega_e = \frac{g_S}{(g_S + g_R)}\omega_{sc} + \frac{R}{n_{im}n_{ri}(g_R + g_S)}\omega_m \quad (20)$$

when the PSS switches to boosting mode the brake opens and the motor has to decrease its own speed by applying some negative torque to increase the supercharger speed. The motor torque and power during the selected interval are shown in Figure 14. The motor torque is the reported value by the motor control unit, and the motor power, P_m , is measured by the AVL battery simulator. The time gap corresponds to a vehicle acceleration, hence the motor is assisting the crankshaft when PSS is in torque assist mode (positive motor torque). When switching to boosting mode the motor initially applies some negative torque to speed up the supercharger and then the motor torque is controlled to track the desired intake manifold pressure, and finally when boosting is not required the motor speed increases by applying a positive torque and when the motor speed is high enough (supercharger speed close to

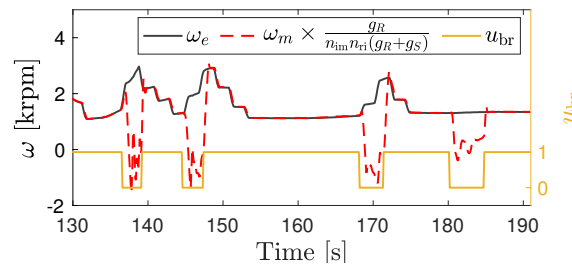


Figure 13. Engine and motor speed for the hardware-in-the-loop experiments during $t = 130$ s to $t = 190$ s

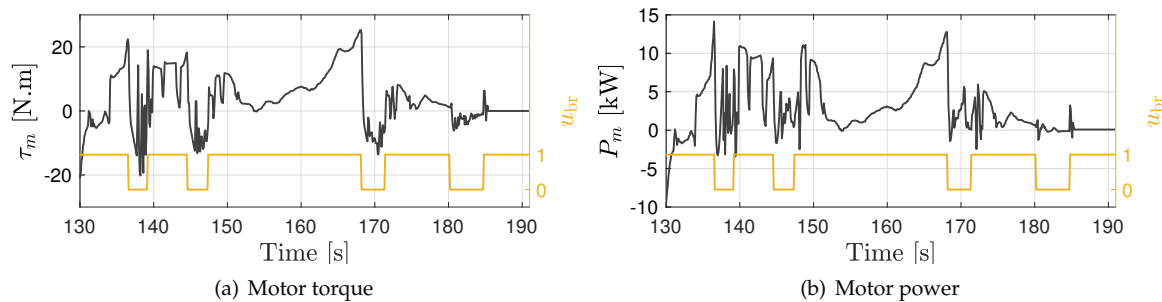


Figure 14. Motor operation for the hardware-in-the-loop experiments during $t = 130$ s to $t = 190$ s (a) motor torque, (b) motor power.

zero) the supercharger is locked again. The brake position is also shown on these plots to distinguish between boosting and torque assist modes. Note that the motor power sign depends on both its torque and speed signs, because the PSS motor can rotate in both directions.

The final piece of the HIL experiments is controlling the desired engine speed. Figure 15 shows the commanded engine speed and its actual value controller by the dynamometer. As seen the dynamometer can perfectly track the desired engine speed.

6. Conclusions

This work presented optimal energy management and hardware-in-the loop experiments for a novel low-voltage hybrid system that can be used either as a flexible supercharger or as a parallel hybrid system, enabling start-stop, regenerative braking, and torque assist. An adaptive equivalent consumption minimization strategy from the literature was modified and customized to the PSS system for selecting both the device mode and the power split ratio in hybrid mode. It was shown that when the relative cost of the electric power is higher, the algorithm chooses to use the supercharger across a wider range of operating points, while when the electric power is relatively cheaper the energy management system supplies the motor torque directly to the engine crankshaft. The implementation of drive cycle hardware-in-the loop experiments on an engine dynamometer test bed was discussed

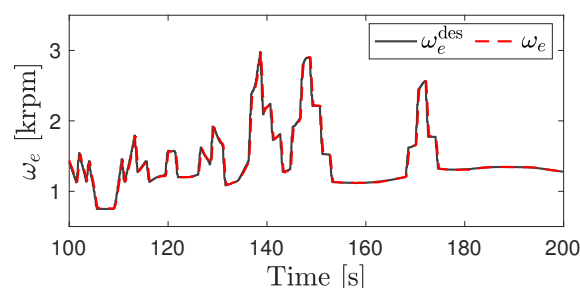


Figure 15. Engine speed and its desired value for the hardware-in-the-loop experiments during $t = 130$ s to $t = 190$ s

in detail and some of practical aspects were explained. It was shown that the new device with the developed energy management system decreases a Ford Escape fuel consumption by 18.4% compared to a baseline turbocharged engine over the FTP75 standard cycle, which is only 4.4% less than the global optimal solution from dynamic programming. Finally, the details of the PSS operation and mode transitions during experiments were shown and discussed in details.

Funding: The information, data, or work presented herein was funded in part by the Advanced Research Projects Agency-Energy (ARPA-E), U.S. Department of Energy, under Award Number DE-AR0000659. The views and opinions of authors expressed herein do not necessarily state or reflect those of the United States Government or any agency thereof.

Acknowledgments: The authors would like to thank the EATON corporation and Southwest Research Institute for providing technical support instrumental to the success of this work.

Abbreviations

The following abbreviations are used in this manuscript:

A-ECMS	Adaptive equivalent consumption minimization strategy
DP	dynamic programming
ECMS	Equivalent consumption minimization strategy
FC	Fuel Consumption
PSS	Power split supercharger
RPECS	Rapid prototyping electronic control system
TC	Torque Converter

References

1. Ehsani, M.; Gao, Y.; Miller, J.M. Hybrid electric vehicles: Architecture and motor drives. *Proceedings of the IEEE* **2007**, *95*, 719–728.
2. Bureau of Transportation Statistics. <https://www.bts.gov/content/gasoline-hybrid-and-electric-vehicle-sales>. Accessed: 2020-03-31.
3. King, J.; Heaney, M.; Saward, J.; Fraser, A.; Criddle, M.; Cheng, T.; Morris, G.; Bloore, P. HyBoost: An Intelligently Electrified Optimised Downsized Gasoline Engine Concept. *Proceedings of the FISITA 2012 World Automotive Congress*. Springer, 2013, pp. 483–496.
4. Volvo. <https://www.volvocars.com>. Accessed: 2020-03-01.
5. Panday, A.; Bansal, H.O. A review of optimal energy management strategies for hybrid electric vehicle. *International Journal of Vehicular Technology* **2014**, *2014*.
6. Enang, W.; Bannister, C. Modelling and control of hybrid electric vehicles (A comprehensive review). *Renewable and Sustainable Energy Reviews* **2017**, *74*, 1210–1239.
7. Gao, J.; Sun, F.; He, H.; Zhu, G.G.; Strangas, E.G. A comparative study of supervisory control strategies for a series hybrid electric vehicle. 2009 Asia-Pacific Power and Energy Engineering Conference. IEEE, 2009, pp. 1–7.
8. Bathaee, S.; Gastaj, A.H.; Emami, S.; Mohammadian, M. A fuzzy-based supervisory robust control for parallel hybrid electric vehicles. 2005 IEEE Vehicle Power and Propulsion Conference. IEEE, 2005, pp. 7–pp.
9. Paganelli, G.; Delprat, S.; Guerra, T.M.; Rimaux, J.; Santin, J.J. Equivalent consumption minimization strategy for parallel hybrid powertrains. *Vehicular Technology Conference*, 2002. VTC Spring 2002. IEEE 55th. IEEE, 2002, Vol. 4, pp. 2076–2081.

10. Borhan, H.; Vahidi, A.; Phillips, A.M.; Kuang, M.L.; Kolmanovsky, I.V.; Di Cairano, S. MPC-based energy management of a power-split hybrid electric vehicle. *IEEE Transactions on Control Systems Technology* **2012**, *20*, 593–603.
11. Lin, C.C.; Peng, H.; Grizzle, J. A stochastic control strategy for hybrid electric vehicles. American Control Conference, 2004. Proceedings of the 2004. IEEE, 2004, Vol. 5, pp. 4710–4715.
12. Lin, C.C.; Peng, H.; Grizzle, J.W.; Kang, J.M. Power management strategy for a parallel hybrid electric truck. *IEEE transactions on control systems technology* **2003**, *11*, 839–849.
13. Nazari, S.; Siegel, J.B.; Stefanopoulou, A. Optimal Energy Management for a Mild Hybrid Vehicle with Electric and Hybrid Engine Boosting Systems. *IEEE Transactions on Vehicular Technology* **2019**.
14. Nazari, S.; Middleton, R.; Siegel, J.; Stefanopoulou, A. Equivalent Consumption Minimization Strategy for a Power Split Supercharger. Technical report, SAE Technical Paper, 2019-01-1207.
15. Nazari, S.; Middleton, R.; Sugimori, K.; Siegel, J.; Stefanopoulou, A. Assessing a hybrid supercharged engine for diluted combustion using a dynamic drive cycle simulation. *SAE International Journal of Alternative Powertrains* **2018**, *7*, 351–368.
16. Nazari, S.; Middleton, R.; Sugimori, K.; Siegel, J.; Stefanopoulou, A. Assessing a Hybrid Supercharged Engine for Highly Diluted Combustion Using a Dynamic Drive Cycle Simulation. Technical report, SAE Technical Paper, 2018-01-0969.
17. Nazari, S.; Siegel, J.; Stefanopoulou, A. Optimal energy management for a hybrid electric vehicle with a power split supercharger. 2018 IEEE Vehicle Power and Propulsion Conference (VPPC). IEEE, 2018, pp. 1–6.
18. Paganelli, G.; Tateno, M.; Brahma, A.; Rizzoni, G.; Guezennec, Y. Control development for a hybrid-electric sport-utility vehicle: strategy, implementation and field test results. American Control Conference, 2001. Proceedings of the 2001. IEEE, 2001, Vol. 6, pp. 5064–5069.
19. Onori, S.; Serrao, L. On Adaptive-ECMS strategies for hybrid electric vehicles. Proceedings of the international scientific conference on hybrid and electric vehicles, Malmaison, France, 2011, Vol. 67.
20. Sun, C.; Sun, F.; He, H. Investigating adaptive-ECMS with velocity forecast ability for hybrid electric vehicles. *Applied energy* **2017**, *185*, 1644–1653.